JACS
JOURNAL OF THE AMERICAN CHEMICAL SOCIETY
Communication
pubs.acs.org/JACS

Solvent-Induced Oriented Attachment Growth of Air-Stable Phase-Pure Pyrite FeS_2 Nanocrystals

Bin-Bin Yu,[†] Xing Zhang,[†] Yan Jiang,[†] Jie Liu,[†] Lin Gu,[‡] Jin-Song Hu,*[,†] and Li-Jun Wan*[,†]

[†]Beijing National Laboratory for Molecular Sciences, CAS Key Laboratory of Molecular Nanostructure and Nanotechnology, Institute of Chemistry, Chinese Academy of Sciences, Beijing 100190, People's Republic of China

[‡]Institute of Physics, Chinese Academy of Sciences, Beijing 100190, People's Republic of China

Supporting Information

ABSTRACT: We report here the selective synthesis of air-stable phase-pure pyrite FeS_2 nanocubes, spheroidal nanocrystals, and microspheres by solvent-induced oriented attachment (OA). It was found that the solvents could control the OA process and thus the morphologies of the products. Solvent exchange experiments and detailed Raman analysis revealed that 1-octanol contributed to the long-term stability of these pyrite nanomaterials.

Pyrite iron disulfide (FeS_2), an eco-friendly material composed of low-cost earth-abundant elements, has attracted much attention in recent years, showing promise for applications in solution-processed photovoltaics, photoelectrochemical cells, and broad spectral photodetectors.[1−4] It has a suitable band gap (E_g = 0.95 eV), a high light absorption coefficient ($\alpha > 10^5$ cm^{-1} for $h\nu > 1.3$ eV),[5] and an adequate minority carrier diffusion length (100−1000 nm) for use as a solar absorber in thin-film solar cells.[6] Considerable effort has been directed toward the synthesis of FeS_2 nanoparticles,[7,8] nanowires,[9] nanoplates,[10] and nanocubes.[11−14] Pyrite thin films have been fabricated by solution- and gas-phase methods.[15−17] However, difficulties in the synthesis of phase-pure pyrite FeS_2 due to the coexistence of impurity phases (FeS, Fe_3S_4, marcasite FeS_2) and its instability in air due to surface decomposition resulted in the power conversion efficiencies (PCEs) of solar cells based on pyrite being less than ∼3%, which is much lower than the PCEs of solar cells based on other chalcogenides, such as CdTe, CIGS, and CZTS.[18,19] Therefore, the key challenge for the application of pyrite in solution-processed solar cells is the synthesis of phase-pure pyrite with a controlled surface state to inhibit its decomposition in air.[7,13,14]

Among the mechanisms that govern the crystal growth, oriented attachment (OA) has been recognized as an interesting and important mechanism.[20−25] The essence of OA is that molecular clusters and nanoparticles attach and aggregate in identical crystallographic orientations, driven by strong, highly direction-specific interactions to merge into a larger single crystal.[20] OA growth of nanomaterials has been reported in a few cases, including PbS nanocrystals (NCs), two-dimensional PbS nanosheets, and linear or zigzag PbSe one-dimensional nanostructures.[22−24] Recently, Li et al. investigated the alignment process and attachment mechanism of OA by direct observation.[25] Although much progress has been made in this field, the alignment process and attachment mechanism in OA have not been fully established. Any new insight into OA will contribute to our understanding of its mechanism and thus guide the synthesis of nanomaterials through this route.

Here, we report the synthesis of air-stable and phase-pure pyrite FeS_2 nanostructures through OA in a facile one-step solvothermal process. It was interestingly found that the OA kinetics and arrangement of FeS_2 primary clusters are closely related to the solvent used in the reaction. Nanocubes of ∼150 nm, spheroidal NCs of ∼50 nm, and microspheres assembled from nanoparticles can be selectively prepared by OA in different solvents. Although all three as-synthesized products are phase-pure pyrite, Raman spectroscopy analysis over time showed that they exhibited distinct stability in air. Both spheroidal FeS_2 NCs and microspheres were stable in air for at least 1 year. After the reason for their stability was understood, air-stable FeS_2 nanocubes were also obtained after solvent exchange.

FeS_2 nanostructures were typically synthesized by using Fe_2O_3 as iron source, sulfur powder as sulfur source, and 1-octylamine or 1-octanol as solvent in a stainless steel autoclave under solvothermal conditions. Detailed synthetic procedures are presented in the Supporting Information. The product synthesized with a 1:1 mixture of 1-octylamine and 1-octanol as mixed solvent was first analyzed by X-ray diffraction (XRD). All diffraction peaks in the XRD pattern (blue curve in Figure 1a) can be well indexed to pyrite FeS_2 (JCPDS no. 42-1340). No signals from marcasite, greigite, pyrrhotite FeS_2, or other impurities were identified. Raman spectroscopy is more sensitive than XRD to detect trace amount of impurities and noncrystalline substances. Figure 1b presents the Raman spectrum of the product (blue curve). The peaks at 340, 378, and 426 cm^{-1} can be well attributed to Raman vibrations of pyrite FeS_2.[14] No any other peaks from impurities, including other iron sulfide phases (FeS, Fe_3S_4, FeS_2, etc.), were detected. These results revealed that the synthesized product was phase-pure pyrite FeS_2. The transmission electron microscopy (TEM) image in Figure 1c shows that the product was spheroidal nanoparticles of oblate or irregular spherical shape. The continuous lattice fringes throughout the whole region of the particle in the high-resolution TEM (HRTEM) image (Figure S1) reveal the

Received: December 22, 2014
Published: February 3, 2015

DOI: 10.1021/ja512979y
J. Am. Chem. Soc. 2015, 137, 2211−2214

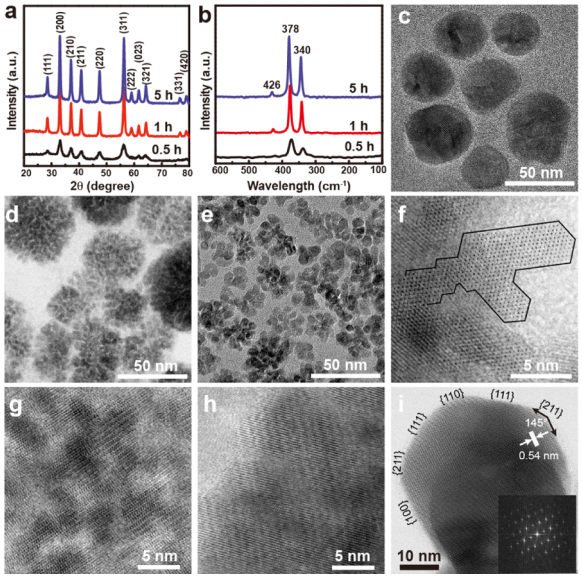

Figure 1. (a) XRD patterns and (b) Raman spectra of the products collected at different times. TEM images of pyrite FeS_2 NCs collected at different times: (c) 5 h, (d) 0.5 h, and (e) 1 h. ABF images demonstrating the different stages of oriented attachment: (f) the initial collision and attachment of FeS_2 primary clusters; (g) imperfect FeS_2 NC with coherent particle−particle interface; (h) FeS_2 NC with continuous lattice fringes but defects; and (i) recrystallization into a perfect single NC. Inset is the corresponding FFT image.

single-crystalline nature of these nanoparticles. The 0.54 nm spacing of the lattice fringes was consistent with the distance of (100) crystallographic planes in pyrite FeS_2. Therefore, the results of XRD, Raman, and TEM analyses exhibited that the product synthesized in 1:1 of 1-octylamine:1-octanol was phase-pure single-crystalline pyrite FeS_2 NCs.

A contrast difference was noted in some NCs in the TEM image (Figure 1c), and defects or voids were occasionally observed in a few NCs (as marked with red arrows in Figure S1), which implied that the growth of these NCs might follow the OA mechanism. In order to reveal the growth process of these pyrite NCs, time-dependent experiments were carried out, and the samples collected at different times were studied by XRD, Raman spectroscopy, and aberration-corrected scanning transmission electron microscopy (STEM) using annular bright-field (ABF) and high-angle annular dark-field (HAADF) detectors. Both XRD patterns (Figure 1a) and Raman spectra (Figure 1b) evidenced that the product collected at 0.5 and 1 h exhibited exclusively the features of pure pyrite FeS_2. Despite the lower intensity of XRD and Raman signals, the product collected at 0.5 h exhibited wider XRD peaks than that collected at 5 h, indicating that the crystal size increased with the increase in reaction time, which is consistent with TEM observations. The ABF (Figure 1d) and HAADF (Figure S2) TEM images indicated that the products collected at 0.5 h were composed of spheroidal flower-like particles of tens of nanometers, which were incompactly assembled from many smaller nanoparticles of several nanometers. The image at higher resolution (Figure S2c) showed that each of these nanoparticles had a clear lattice fringe, and the nanoparticles attached together in a certain orientation. As the reaction time increased, the small nanoparticles merged into larger NCs (Figure 1e), which attached to each other to form large aggregates, and eventually grew into well-crystallized NCs of tens of nanometers (Figure 1c). These results supported that the growth of FeS_2 NCs in this experiment should follow the OA mechanism. To further illuminate the growth process, a series of ABF TEM images are shown in Figure 1f−i. The atomic-resolution TEM image in Figure 1f clearly demonstrates the initiation of FeS_2 primary NCs and their oriented aggregation driven by the decrease in the surface and grain boundaries' free energies. Figure 1g presents the primary NCs linked together in an aligned crystallographic arrangement. The parallel and coherent lattice fringes throughout the whole region indicate that all primary NCs shared the same crystallographic orientation and constructed an imperfect larger crystal. As the reaction proceeded, the lattice fringes became clearer and more continuous (Figure 1h). The decrease in the defects and the elimination of interspaces among primary NCs reflected the process of orientation and crystallization. After completion of the growth, a well-crystallized single crystal was formed of a size slightly smaller than the size of the initial aggregates of the primary NCs (Figure 1d). The clear and continuous lattice fringes in whole particle region shown in Figures 1i and S3, as well as the two-dimensional spot array in the FFT image (inset in Figure 1i), reveal that the final nanoparticle has a perfect single crystalline structure.

Moreover, it was interestingly found that the OA process and the sizes and morphologies of the products were strongly dependent on the solvents used in the synthesis. When only 1-octylamine was used as the solvent and reducing agent, nanocubes of ∼150 nm were obtained (Figure 2a). A HRTEM image indicated that these nanocubes were single crystals (Figure S4). Traces of NC agglomeration appeared in some nanocubes (marked with arrows in Figure S5), and time-dependent experiments (Figure S5) revealed that these nanocubes were formed through the OA mechanism. When 1-octanol was added in a volume ratio of 2:1 for 1-octylamine:

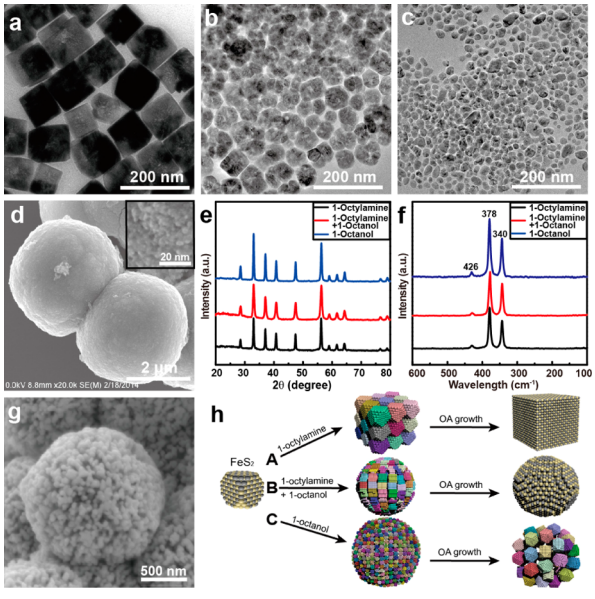

Figure 2. TEM images of FeS_2 products prepared with solvents of 1-octylamine and 1-octanol in different volume ratios: (a) 12:0, (b) 8:4, and (c) 6:6. SEM images of the pyrite FeS_2 microspheres prepared in pure 1-octanol after reaction for (d) 5 h and (g) 36 h. (e) XRD patterns and (f) Raman spectra of FeS_2 products prepared in different solvents. (h) Schematic illustration of the formation of FeS_2 nanocubes, spheroidal NCs, and microspheres (not in scale).

DOI: 10.1021/ja512979y
J. Am. Chem. Soc. 2015, 137, 2211−2214

1-octanol, the morphology of the product started to change from nanocube to spheroidal nanoparticle, and the particle size shrank to ~100 nm (Figure 2b). As the amount of 1-octanol was increased, giving 1:1 1-octylamine:1-octanol, the particle changed to an oblate or irregular spheroidal shape, and the size further decreased to ~50 nm (Figure 2c). When 1-octanol was used only as the solvent, microspheres of ~3 μm were obtained instead (Figure 2d). A high-resolution SEM image (inset) displayed that the microspheres were compactly assembled from plenty of nanoparticles, each several nanometers in size. The XRD patterns (Figure 2e) and Raman spectra (Figure 2f) confirmed that all products were phase-pure pyrite FeS_2, although they had completely different morphologies. Moreover, it should be noted that the growth time of the final structures in these experiments was also related to the solvent used. In the case of 1-octylamine as solvent, the attachment and crystallization of primary NCs happened fast. The final nanocubes formed in 1 h and did not change after then (Figure S5). When the mixed solvent of 1:1 1-octylamine:1-octanol was used instead, the formation of spheroidal NCs took ~2 h, and the NCs were unchanged after that (Figure S6). When 1-octanol was used as the solvent, the attachment of nanoparticles took a much longer time. Fe_2O_3, as the raw material, was present in the reaction system after 4 h of reaction. After another 1 h, Fe_2O_3 was completely converted into FeS_2 microspheres assembled from nanoparticles (Figure S7). When the reaction time was extended to 36 h, the microspheres compactly assembled from small nanoparticles evolved into microspheres composed of bigger NCs with apparent voids between them (Figure 2g), indicating that the small nanoparticles grew into larger ones through OA. These results revealed that the OA and crystal growth in this system were closely related to the used solvent. Figure 2h depicts the OA processes in the typical cases with different solvents. In the case of 1-octylamine as solvent (path A), the preferential adsorption of 1-octylamine on {100} facets resulted in the formation of nanocubes through OA of FeS_2 primary NC seeds.[8] When 1-octanol was introduced, the preferential adsorption of 1-octylamine was neutralized, leading to the formation of spheroidal FeS_2 NCs after OA (path B). The higher reactivity of 1-octylamine as reducing agent and stronger driving force for OA caused the higher OA growth rate at higher concentrations of 1-octylamine, and thus the faster growth and larger size of nanocubes than spheroidal NCs. In the case of pure 1-octanol as solvent, it took longer a time to completely convert Fe_2O_3 into FeS_2 due to the lower reactivity of 1-octanol as reducing agent. The as-grown FeS_2 nanoparticles of several nanometers subsequently aggregated into microspheres in 1-octanol to minimize the surface energy before they grew into larger NCs due to the relatively weak driving force for OA growth in 1-octanol. After aging for longer time, these small attached nanoparticles recrystallized into larger NCs and left spaces in the microsphere (path C).

The preparation of air-stable FeS_2 nanomaterials is essential for their application but still challenging because their surface is not stable thermodynamically and susceptible to oxidation. In this study, it was found that FeS_2 NCs synthesized with different solvents exhibited different air stability. Although the XRD patterns of three samples prepared with 1-octylamine, 1:1 1-octylamine:1-octanol, and 1-octanol did not show obvious differences after exposure to air for 2 months, the Raman spectra of FeS_2 nanocubes prepared with 1-octylamine clearly displayed two new Raman peaks at 213 and 282 cm^{-1}, while the other two samples did not (Figure S8). This indicated that the surface states of the nanocubes changed after exposure to air, although their main bodies still had the crystalline structure of pyrite. Detailed Raman analysis over time (Figures 3a and S9)

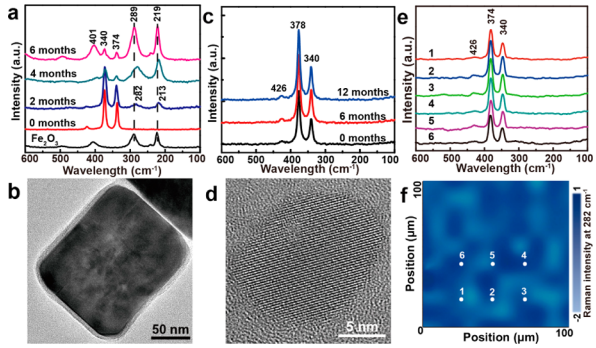

Figure 3. Raman spectra of FeS_2 nanocubes (a) and spheroidal NCs (c) after being stored in air for different times. (b) TEM image of a FeS_2 nanocube and a FeS_2 spheroidal NC (d) after exposure to air for 3 months. (e) Raman mapping spectra of spheroidal FeS_2 NCs after being stored in air for 12 months and (f) the corresponding mapping image at 282 cm^{-1}.

showed that the Raman vibrations at 213 and 282 cm^{-1}, which could be well attributed to FeS, appeared after the 2-month air exposure. New Raman peaks at 219, 289, 401, 496, 604, and 1305 cm^{-1} etc., which could be well attributed to hematite Fe_2O_3, appeared after 6 months of air exposure. The intensities of these peaks increased over time and dominated in the spectrum after 6 months of air exposure, implying that the surfaces of the FeS_2 nanocubes were oxidized to Fe_2O_3. TEM observation (Figure 3b) exhibited that the surface of the crystalline nanocubes was coated with an amorphous layer ~10 nm thick after 3 months of air exposure, which further confirmed the surface change of the nanocubes. On the other hand, the Raman spectra of spheroidal FeS_2 NCs and microspheres did not change even after 12 months of air exposure, as shown in Figures 3c and S10, respectively. TEM images corroborated that no change in size or morphology was observed for spheroidal NCs and their surface did not show any change after air exposure as well (Figures 3d and S11). For further investigation of its stability in air, Raman mapping was conducted on the film of spheroidal FeS_2 NCs. None of the Raman spectra (Figure 3e) recorded at six different locations (randomly selected in the region shown in Figure 3f) after 12 months of air exposure showed any features from impurities. Raman imaging at 282 cm^{-1}, which is the typical Raman vibration of FeS impurity, showed that the signals on the whole region of 100 × 100 μm were at the baseline level. This result revealed that the film of the synthesized spheroidal FeS_2 NCs was stable in air.

Furthermore, in order to understand why the spheroidal FeS_2 NCs synthesized with the 1:1 mixture of 1-octylamine and 1-octanol were stable in air while FeS_2 nanocubes were not, the effect of solvents on the stability was investigated by taking FeS_2 nanocubes for an example. In brief, after synthesis in 1-octylamine, the FeS_2 nanocubes suspension was divided into three equal portions. Two portions were centrifuged, washed, and redispersed in a 1:1 mixture of 1-octylamine and 1-octanol, and in 1-octanol, respectively, for 5 h. The three samples were washed, dried, and stored in parallel in air for 3 months and then subjected to Raman mapping. As shown in Figure 4a,b,

DOI: 10.1021/ja512979y
J. Am. Chem. Soc. 2015, 137, 2211−2214

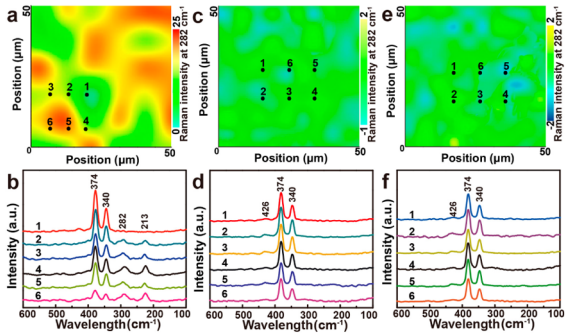

Figure 4. Raman mapping images of nanocubes after 3 months of air exposure and the spectra recorded at the locations marked on the corresponding top images: (a,b) without solvent exchange, (c,d) treated with mixed solvent of 1-octylamine and 1-octanol, and (e,f) treated with 1-octanol.

Raman mapping on a randomly selected 50 × 50 μm area and the corresponding spectra recorded at six points marked in Figure 4a showed clear Raman signals from impurities in the sample without solvent exchange. The sample with the mixed solvent exchange exhibited uniform Raman signals throughout the whole area and no peaks other than the ones from pyrite FeS_2 (Figure 4c,d). No changes in the Raman mapping and spectra were found on the sample treated with 1-octanol as well (Figure 4e,f). Similar experiments were also carried out by using the supernatants in the synthesis of spheroidal FeS_2 NCs and microspheres as the exchange solvent. It was found that FeS_2 nanocubes were stable for 3 months of air exposure after solvent exchange with both supernatants, as indicated by the Raman analysis (Figure S12). These results revealed that 1-octanol played a crucial role in stabilizing FeS_2 nanomaterials in our experiments. Stable FeS_2 nanocubes can be prepared by synthesizing nanocubes in pure 1-octylamine and then treating them with the solvent containing 1-octanol.

In summary, the phase-pure and air-stable pyrite FeS_2 NCs, nanocubes, and self-assembled porous microspheres can be selectively synthesized through oriented attachment. It was interestingly found that the process of the OA of FeS_2 primary clusters is closely related to the solvent in the system, which controlled the morphologies of the final FeS_2 nanostructures. Detailed Raman experiments over time further disclosed that the 1-octanol solvent was responsible for the long-term stability of these materials. These findings will contribute to the understanding of crystal growth via OA as well as to the preparation of stable FeS_2 nanomaterials for different applications.

■ ASSOCIATED CONTENT

Supporting Information

Detailed experimental description; Supplementary TEM and HRTEM images; XRD and Raman analyses. This material is available free of charge via the Internet at http://pubs.acs.org.

■ AUTHOR INFORMATION

Corresponding Authors

*hujs@iccas.ac.cn

*wanlijun@iccas.ac.cn

Notes

The authors declare no competing financial interest.

■ ACKNOWLEDGMENTS

We acknowledge financial support from the National Key Project on Basic Research (Grants Nos. 2015CB932302 and 2011CB808701), the National Natural Science Foundation of China (Grants Nos. 91127044 and 21173237), and the Strategic Priority Research Program of the Chinese Academy of Sciences (Grant No. XDB12020100).

■ REFERENCES

(1) Wang, Y. C.; Wang, D. Y.; Jiang, Y. T.; Chen, H. A.; Chen, C. C.; Ho, K. C.; Chou, H. L.; Chen, C. W. *Angew. Chem., Int. Ed.* **2013**, *52*, 6694.

(2) Ennaoui, A.; Fiechter, S.; Pettenkofer, C.; Alonso-Vante, N.; Büker, K.; Bronold, M.; Höpfner, C.; Tributsch, H. *Sol. Energy Mater. Sol. Cells* **1993**, *29*, 289.

(3) Gong, M.; Kirkeminde, A.; Xie, Y.; Lu, R.; Liu, J.; Wu, J. Z.; Ren, S. *Adv. Opt. Mater.* **2013**, *1*, 78.

(4) Wang, D. Y.; Jiang, Y. T.; Lin, C. C.; Li, S. S.; Wang, Y. T.; Chen, C. C.; Chen, C. W. *Adv. Mater.* **2012**, *24*, 3415.

(5) Altermatt, P. P.; Kiesewetter, T.; Ellmer, K.; Tributsch, H. *Sol. Energy Mater. Sol. Cells* **2002**, *71*, 181.

(6) Ennaoui, A.; Tributsch, H. *Sol. Energy Mater.* **1986**, *14*, 461.

(7) Puthussery, J.; Seefeld, S.; Berry, N.; Gibbs, M.; Law, M. *J. Am. Chem. Soc.* **2010**, *133*, 716.

(8) Gong, M.; Kirkeminde, A.; Ren, S. *Sci. Rep.* **2013**, *3*, 2092.

(9) Cabán-Acevedo, M.; Faber, M. S.; Tan, Y.; Hamers, R. J.; Jin, S. *Nano Lett.* **2012**, *12*, 1977.

(10) Kirkeminde, A.; Ruzicka, B. A.; Wang, R.; Puna, S.; Zhao, H.; Ren, S. *ACS Appl. Mater. Interfaces* **2012**, *4*, 1174.

(11) Bai, Y.; Yeom, J.; Yang, M.; Cha, S.-H.; Sun, K.; Kotov, N. A. *J. Phys. Chem. C* **2013**, *117*, 2567.

(12) Lucas, J. M.; Tuan, C.-C.; Lounis, S. D.; Britt, D. K.; Qiao, R.; Yang, W.; Lanzara, A.; Alivisatos, A. P. *Chem. Mater.* **2013**, *25*, 1615.

(13) Macpherson, H. A.; Stoldt, C. R. *ACS Nano* **2012**, *6*, 8940.

(14) Bi, Y.; Yuan, Y.; Exstrom, C. L.; Darveau, S. A.; Huang, J. *Nano Lett.* **2011**, *11*, 4953.

(15) Seefeld, S.; Limpinsel, M.; Liu, Y.; Farhi, N.; Weber, A.; Zhang, Y.; Berry, N.; Kwon, Y. J.; Perkins, C. L.; Hemminger, J. C.; Wu, R.; Law, M. *J. Am. Chem. Soc.* **2013**, *135*, 4412.

(16) Berry, N.; Cheng, M.; Perkins, C. L.; Limpinsel, M.; Hemminger, J. C.; Law, M. *Adv. Energy Mater.* **2012**, *2*, 1124.

(17) Morrish, R.; Silverstein, R.; Wolden, C. A. *J. Am. Chem. Soc.* **2012**, *134*, 17854.

(18) Green, M. A.; Emery, K.; Hishikawa, Y.; Warta, W.; Dunlop, E. D. *Prog. Photovoltaics Res. Appl.* **2012**, *20*, 12.

(19) Mitzi, D. B.; Yuan, M.; Liu, W.; Kellock, A. J.; Chey, S. J.; Deline, V.; Schrott, A. G. *Adv. Mater.* **2008**, *20*, 3657.

(20) Penn, R. L.; Banfield, J. F. *Science* **1998**, *281*, 969.

(21) Banfield, J. F.; Welch, S. A.; Zhang, H.; Ebert, T. T.; Penn, R. L. *Science* **2000**, *289*, 751.

(22) Cho, K.-S.; Talapin, D. V.; Gaschler, W.; Murray, C. B. *J. Am. Chem. Soc.* **2005**, *127*, 7140.

(23) Yin, Y.; Alivisatos, A. P. *Nature* **2005**, *437*, 664.

(24) Schliehe, C.; Juarez, B. H.; Pelletier, M.; Jander, S.; Greshnykh, D.; Nagel, M.; Meyer, A.; Foerster, S.; Kornowski, A.; Klinke, C. *Science* **2010**, *329*, 550.

(25) Li, D.; Nielsen, M. H.; Lee, J. R.; Frandsen, C.; Banfield, J. F.; De Yoreo, J. J. *Science* **2012**, *336*, 1014.

DOI: 10.1021/ja512979y
J. Am. Chem. Soc. 2015, 137, 2211−2214